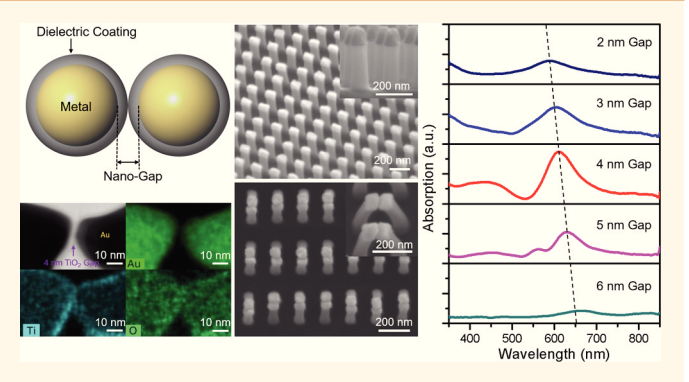




Probing Gap Plasmons Down to Subnanometer Scales Using Collapsible Nanofingers

Boxiang Song, [†] Yuhan Yao, [†] Roelof E. Groenewald, [‡] Yunxiang Wang, [†] He Liu, [†] Yifei Wang, [†] Yuanrui Li, [†] Fanxin Liu, ^{||} Stephen B. Cronin, [†] Adam M. Schwartzberg, [§] Stefano Cabrini, [§] Stephan Haas, [‡] and Wei Wu*, [†]

ABSTRACT: Gap plasmonic nanostructures are of great interest due to their ability to concentrate light into small volumes. Theoretical studies, considering quantum mechanical effects, have predicted the optimal spatial gap between adjacent nanoparticles to be in the subnanometer regime in order to achieve the strongest possible field enhancement. Here, we present a technology to fabricate gap plasmonic structures with subnanometer resolution, high reliability, and high throughput using collapsible nanofingers. This approach enables us to systematically investigate the effects of gap size and tunneling barrier height. The experimental results are consistent with previous findings as well as with a straightforward theoretical model that is presented here.



KEYWORDS: gap plasmon, nanofingers, quantum effects, plasmonics, nanoimprint lithography

lasmonic nanostructures have many fascinating properties. For example, they can focus light energy onto a small volume at nanometer scales. 1-6 This feature makes them a promising platform for various applications, including optical communication, disease diagnosis, and chemical sensing.9 One class of the most intriguing plasmonic nanostructures is that of nanoparticle pairs with small interparticle gaps, because it can create strong field enhancement at a hot spot between the two particles. 6,10-13 It has been theoretically predicted that the optimal hot spot is a subnanometer gap between two metallic particles, 14-18 considering both classical electromagnetic theory and quantum mechanical effects. While many attempts have been made in recent years to fabricate gap plasmonic nanostructures with sub-5 nm gaps, ^{19–24} the limitation of traditional fabrication techniques poses serious obstacles to reliably producing precisely controllable nanogaps with high throughput. In order to experimentally investigate these theoretical predictions of optimal gap size and design such structures for practical applications, one needs to demonstrate accurately controlled gap size in large periodic nanogap arrays. Moreover, it is important to understand electron tunneling across the gap in

such structures, as this appears to be a key mechanism in controlling plasmonic enhancement.

Here we present a technology to fabricate large-area gapped plasmonic structures deterministically with atomic precision, high throughput and high reliability at low cost. The technology is based on collapsible nanofingers fabricated using nanoimprint lithography (NIL), reactive-ion etch (RIE), and atomic layer deposition (ALD). Figure 1 shows a schematic illustration of such a gap plasmonic nanostructure. A pair of metallic nanoparticles is placed on top of two nanofingers in flexible polymer (i.e., nanoimprint resist) with high aspect ratio. Atomic layer deposition is then used to coat a thin conformal dielectric layer. The ALD-coated dielectric layer serves as the spacer to define the spatial gaps between the metallic particles. By collapsing the pair of nanofingers, two metallic nanoparticles with dielectric coating contact each other. Therefore, the gap size between two metallic nanoparticles is well-defined by twice the thickness of the ALD-coated dielectric layers. Since the

Received: March 1, 2017 Accepted: June 9, 2017 Published: June 9, 2017

[†]Ming Hsieh Department of Electrical Engineering, University of Southern California, Los Angeles, California 90089, United States

[‡]Department of Physics and Astronomy, University of Southern California, Los Angeles, California 90089, United States

[§]Molecular Foundry, Lawrence Berkeley National Laboratory, Berkeley, California 94720, United States

Department of Applied Physics, Zhejiang University of Technology, Hangzhou, Zhejiang 310023, China

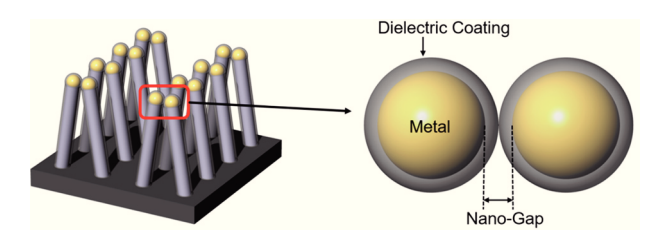


Figure 1. Schematic of controllable hot spots created using nanofingers. A pair of metallic nanoparticles with ALD-coated dielectric layers contact each other when flexible nanofingers beneath them collapse. The spatial gap size is defined by twice the dielectric layer thickness, and the hot spot is at the gap center.

ALD process deposits dielectric film atomic-layer-by-atomic-layer with high conformity, 25-27 atomic precision on gap thickness control is achieved. The small separation ensures strong coupling between each pair of metallic nanoparticles, such that the hot spot with greatly enhanced electromagnetic near-field is located within the dielectric nanogap.

Moreover, the tunneling barrier heights for electrons can also be controlled by using appropriate spacer materials, ²⁸ which strongly affect the plasmonic enhancement. We have characterized the plasmonic enhancement characterized with UV-Vis-NIR spectrophotometers by measuring the absorption spectra of different samples. The evolution of the absorption peak as a function of gap size for different dielectric gap materials was analyzed. We successfully detected optimal gap sizes with strongest plasmonic enhancement experimentally. By

using different gap materials, we investigated the effect of tunneling barrier heights. It was found that as the tunneling barrier height is decreased, the enhancement of electron tunneling manifests itself in a wider optimal gap. Moreover, we observed a redshift of the plasmon frequency with increasing gap size when the gaps narrowed to sub-5 nm range.²¹

The fabrication procedure of collapsible gold nanofingers is described schematically in Figure 2 (for details, see Methods Section). First, a mold with grid hole arrays of 200 nm pitch was formed by double interference lithography, as described in previous publications.^{29–31} Then, UV-curable nanoimprint lithography³²⁻³⁵ (NIL) was utilized to transfer the original hole pattern to a polymeric reverse-tone (pillar) daughter mold using a custom-designed nanoimprint machine. UV nanoimprint resist and lift-off underlayer were spin-coated onto glass substrates (Figure 2a). Then subsequent NIL (Figure 2b), residual layer etching, metal evaporation, and lift-off steps were performed to create gold caps array (Figure 2c). As the pattern can be defined precisely by the initial interference lithography and duplicated reliably by NIL, 29 an array of nanofingers can be fabricated uniformly over a large area with high throughput after etching the uncovered UV nanoimprint resist (Figure 2d). In our study, finger arrays over 1.4 in. by 1.4 in. areas were used to guarantee a good signal-to-noise ratio. The samples were then covered by dielectric coatings of variable thickness using ALD process (Figure 2e). Finally, after soaking into ethanol and air-drying, the fingers closed together in a dimer configuration as shown in Figure 2f. The capillary force drove the collapse of nanofingers. A similar mechanism was reported

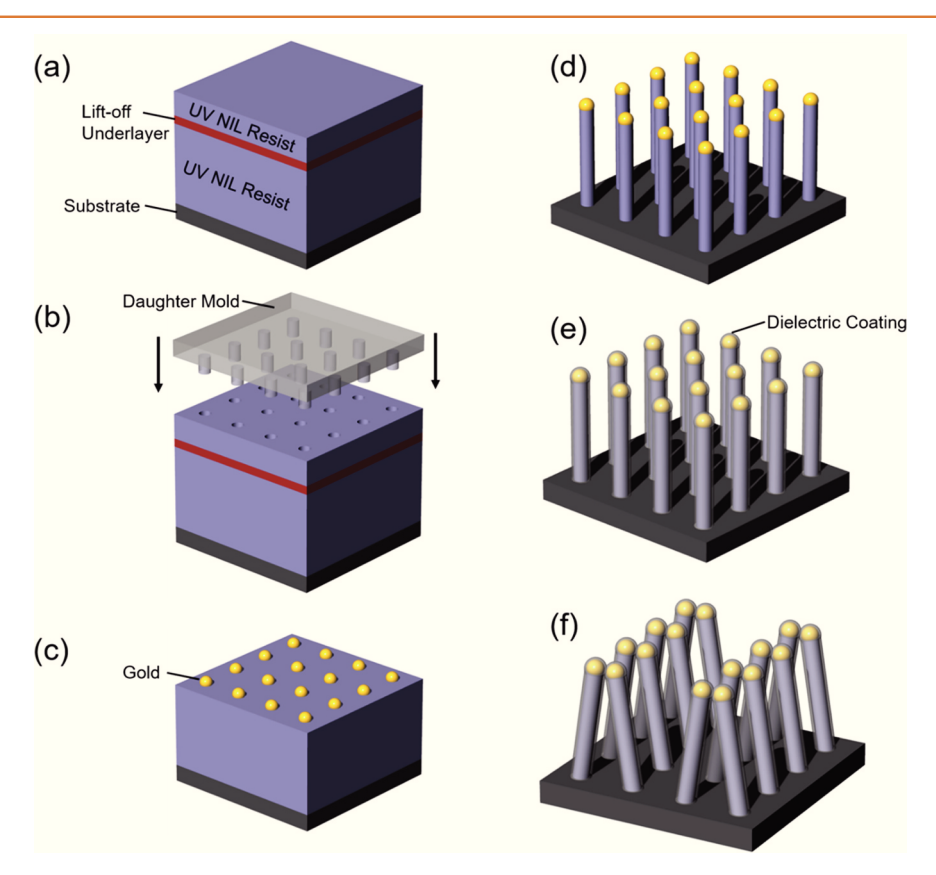


Figure 2. Fabrication procedure of nanofingers: (a) Spin coating and UV curing of 600 nm thick UV NIL resist, then spin coating 100 nm lift-off underlayer and 100 nm UV nanoimprint resist layers. (b) Nanoimprinting using daughter mold. (c) After etching residual layer, metal evaporation, and lift-off, gold caps array was left on the thick UV nanoimprint resist. (d) Etching the underlying UV nanoimprint resist without Au covering. (e) ALD deposition of dielectric films. (f) Soaking and air-drying of the ethanol to induce the collapse of nanofingers.

before.^{36–40} We found that proper aspect ratio and straight sidewalls are necessary for uniform dimer-like finger collapsing. Low aspect ratio or tapered sidewall will prevent the fingers from collapsing, while fingers with aspect ratio too high will result in a random collapse with large number of fingers. Once the nanoparticles touch, they will not separate due to van der Waals forces.³⁶ Figure 3 shows the scanning electron

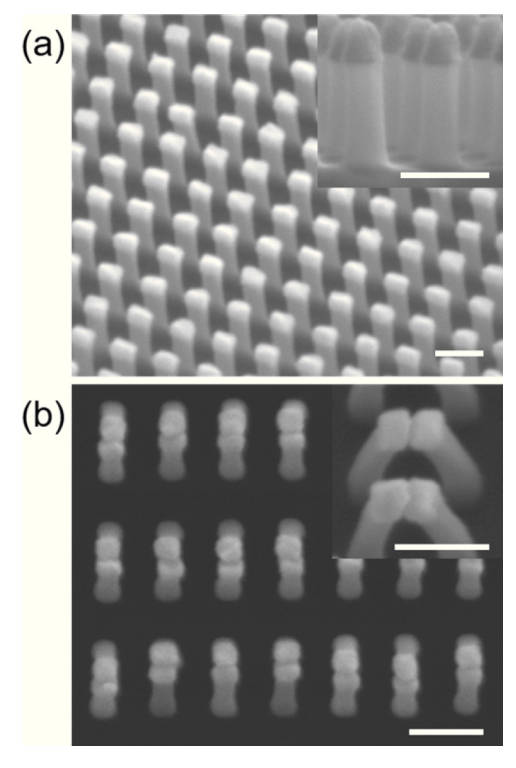


Figure 3. (a) SEM image of nanofingers before collapse. (b) SEM images of nanofingers after collapse. The inset is magnified image of the same nanofingers from a different viewing angle. The diameter and height of each finger are 60 and 350 nm, respectively. Scale bars in the SEM images are 200 nm.

microscopy (SEM) images of nanofingers before and after closing. The diameter and height of each finger is 60 and 350 nm, respectively. Figure 4a shows the transmission microscopy (TEM) image at the nanogap after nanofingers with 2 nm TiO₂ ALD film coating collapsed. In the picture, the gap size is defined as the distance between two closest points of two gold nanoparticles, which is shown as twice the thickness of the ALD film. Corresponding energy-dispersive X-ray spectroscopy (EDS) mappings of Au, Ti, and O are shown in Figure 4b, c, and d. The gap exists in Au EDS mapping while no gap exists in Ti and O EDS mappings. That indicates the Au nanoparticles are uniformly covered by continuous and conformal TiO2 film deposition and the gap size is well-defined by twice the thickness of the TiO2 film.

RESULTS AND DISCUSSION

Surface plasmons are excited in these collapsed nanofingers upon light incidence. By coupling with incident photons, one observes strong enhancement while reradiating the energy. The gap size plays a critical role in tuning this plasmonic enhancement. Based on classical electromagnetic theory, stronger near-field enhancement and a diverging red-shift of bonding plasmon resonance emerges as two nanoparticles

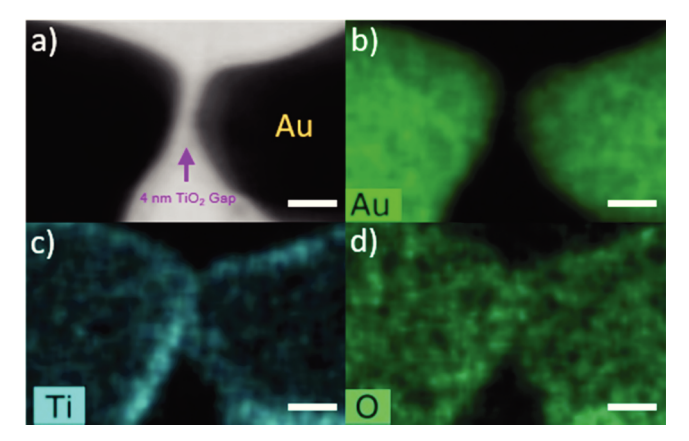


Figure 4. (a) TEM image of the dielectric nanogap in the nanofingers with 2 nm TiO2 coating. (b) EDS mapping of Au in the TEM image. (c) EDS mapping of Ti in the TEM image. (d) EDS mapping of O in the TEM image. Scale bars in the images are 10 nm.

approach each other. However, extensive theoretical studies have shown that for these very narrow gaps at sub-5 nm, several factors can significantly reduce the field enhancement. 14-16,51-53 Quantum mechanical effects become relevant in this regime. They are basically (i) electrons tunneling from one nanostructure to another through the gap, and (ii) the finite spatial profile of the plasmon-induced screening charge (nonlocality). To properly take these effects into consideration, a fully quantum mechanical treatment based on linear quantum calculations predicts that shrinking the gap size will result in stronger tunneling and therefore limited field enhancement for ultrasmall gaps. 54-57 In the dimer-like gap plasmonic structures, bonding dimer plasmon (BDP) originating from the hybridization of the dipolar plasmon modes of individual nanoparticles and charge transfer plasmon (CTP) referring to the electron tunneling between nanoparticles, are the two dominant competing plasmon modes. 14,17 Based on these modes, optimal gap sizes which can provide the strongest enhancement have been predicted theoretically. 14-18

In order to study the plasmonic enhancement of the closed nanofingers, we chose the absorption spectrum as an indicator, which is convenient and straightforward. Figure 5 shows the absorption spectra of the collapsed nanofingers with TiO₂ as the gap material. The gap sizes were chosen as 2, 3, 4, 5, 6 nm, respectively. As the gap size is shrunk from 6 to 4 nm, the peak absorption strength at resonance frequency was observed to increase. This is consistent with the classical electromagnetic prediction. However, when the gap size was reduced from 4 to 2 nm, the peak absorption strength at resonance frequency weakened. This indicates that plasmonic quantum effects deviate the spectral response of the surface plasmon modes from the classical model for TiO2 gap at this scale. It is clear that the 4 nm TiO₂ gap system has the strongest plasmon light absorption. This means the most energy is stored in the surface plasmon, and the strongest near-field enhancement is realized by reradiating the energy. We successfully observed and determined the optimal gap size systematically in experiment. In addition, the absorption peaks exhibit a red shift as the gap size is increased, which is also opposite to classical prediction but agrees with the quantum mechanical calculation. For comparison, perpendicular polarized light was illuminated on samples in the same setup. Figure 6 shows a comparison result for absorption spectra of nanofingers with 4 nm TiO₂ gap. No

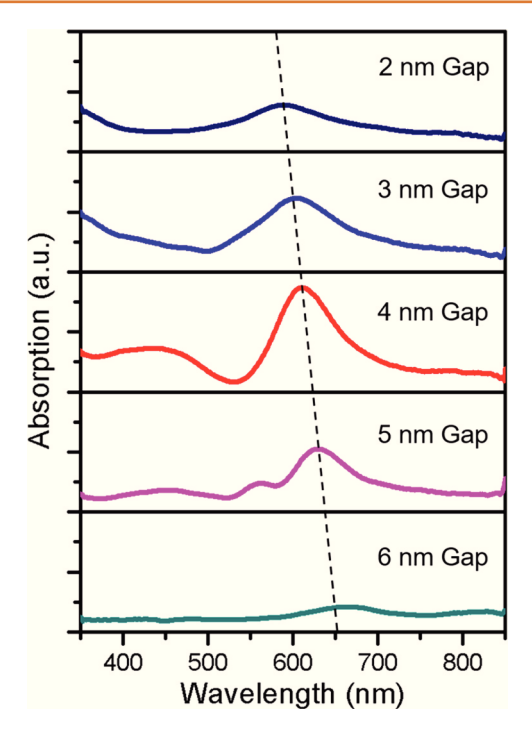


Figure 5. Absorption spectra of collapsed nanofingers with TiO2 as gap material. The gap sizes are 2, 3, 4, 5, 6 nm, respectively.

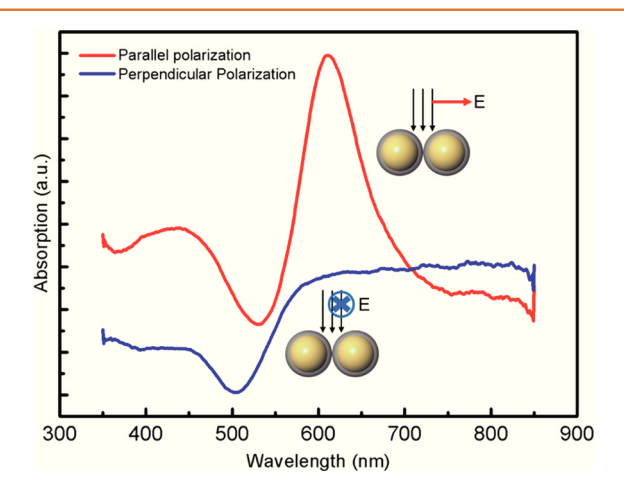


Figure 6. Absorption spectra of collapsed nanofingers by using parallel and perpendicular polarized incident light.

absorption peak is observed if the polarization was perpendicular. Based on previous work reported,²¹ parallel polarized light will primarily excite the longitudinal bonding

dipole plasmon (LBDP) mode, which is generally called BDP in the literature. The absorption peaks of the previous results mainly originate from the combination of LBDP and CTP modes. However, upon the perpendicularly polarized light's illumination, the transverse dipole plasmon (TDP) mode is the dominant mode excited, which originates from the uncoupled dipole in individual nanoparticles. In that case, the nanofinger pairs behave more like isolated monomers rather than dimers, since TDP is perpendicularly polarized with the resonant position and weakly dependent on the gap size. As a result, the absorption strength from TDP is too weak to be observed after the compensation of background signal.

In order to investigate the dependence of plasmonic enhancement on the electron tunneling effect, we used different ALD dielectric materials as the gap material. As the electrons tunnel from one gold nanoparticle to another, the tunneling barrier height, based on energy band diagrams, is defined as the difference between the Fermi energy of gold (5.1 eV) and the electron affinity (EA) of corresponding dielectric materials.²⁸ We chose TiO₂, WO₃, and SiO₂, with electron affinities equal to 4.21, 3.45, and 0.90 eV, respectively, 58-60 so that the corresponding tunneling barrier heights are 0.89, 1.65, and 4.20 eV. With reduced tunneling barrier height, the tunneling strength is enhanced, which is manifested by a wider optimal gap. This is why the observed optimal gap size for TiO₂ gap is much larger than the optimal vacuum gap size theoretically predicted in most of the literature, considering that vacuum holds a 5.1 eV tunneling barrier height. In order to analyze the underlying physics of observed enhancements and redshifts, we plotted the peak absorption strength and the resonance frequency versus the wavelength of incident light for different material, as shown in Figure 7. From the Figure 7a, we identified the optimal gap sizes with strongest plasmonic absorption for different gap materials. We also investigated the red shift of resonance frequency with increasing gap size in Figure 7b. The uncertainties of the peak absorption strength and peak location are caused by the differences between individual samples, including defect level and geometric variance. Triple standard deviation was applied as the error for a confidence interval of 99.7%. They are all within permissible error range.

In order to understand and correlate the experimental observations with quantum based model calculations incorporating electron tunneling and nonlocality, we need a model which can ultimately guide the effective design of potential applications. There have been extensive studies of the optical properties of spherical nanoparticles separated by relatively large distances. ^{61,62} However, these calculations become more

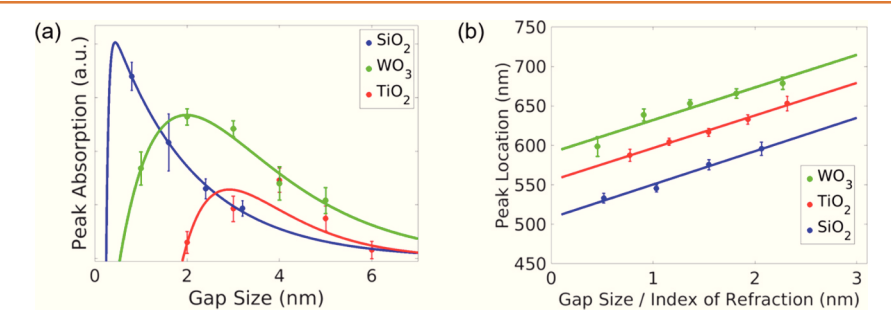


Figure 7. (a) The measured peak absorption for different values of gap size from three different gap materials. The data is fit according to eq 1. (b) The measured red shift of absorption peaks with increasing gap size from three different gap materials. The data is fit according to eq 2.

complicated when the nanoparticles are close to each other, such that light scattered from them exhibits phase coherence. Based on the observation that coherence is responsible for the electro-magnetic hotspot⁶⁴ observed between nanoparticles in this experiment we propose the simple, phenomenological model discussed below to describe the electric field enhancement at the center point between two nanoparticles for different separation distances (D). This model also provides an argument for the observed redshift of the plasmon frequency with increasing separation. It is known that the dominant peak from the electron energy loss spectrum (EELS) of a pair of metallic nanoparticles separated by a small distance is due to the lowest order longitudinal dipole mode⁶⁵ referred to as the bonding dimer plasmon (BDP).66 Classical calculations show the onset of another strong plasmon mode (known as the charge transfer plasmon, CTP) when the nanoparticles touch. 50,67 Quantum calculations show a weakening of the BDP mode with a strengthening of CTP mode at finite separation distances (*i.e.*, D > 0). This is due to quantum mechanical tunneling⁶⁸ allowing charge transfer even without a direct conduction path.

We believe the observations discussed in this article can primarily be attributed to three physical processes. First, the field enhancement seen midway between nanoparticles can be attributed to the strong Coulomb field caused by separated charges on both nanoparticles. The strength of this field depends on the amplitude of the incident field, the dielectric constant of the coating material and various other properties of the system. We call this parameter $q_{\rm eff}$ to stress that it originates from opposite charges coming close to each other due to the longitudinal dipole oscillations on each nanoparticle. Second, quantum mechanical tunneling allows charge transfer between the particles even with a finite D, decreasing the charge separation and consequently also the strength of the field enhancement. In the simplest example, that of 2 quantum wells separated by a barrier of width D, it is a well-known result that the probability of tunneling goes as $e^{-\lambda D}$ where λ is the decay length of the wave function which depends on the barrier height and the particle energy. Applying this simplified approach here we let $q_{\rm eff} \to q_{\rm eff} (1-e^{-\lambda D})$ to account for the loss of charge separation and the consequent weakening of the bonding dimer plasmon due to tunneling. Finally, we have to account for energy loss in the system which occurs through many channels, such as absorption in the dielectric coating and decay of the surface plasmon. For simplicity we modeled this as a simple damping term that depends on the separation between the particles. This is justified since the further the separation, the more coating each particle has, which in turn increases absorption. Thus, we arrived at the following expression to describe the most important processes affecting the strength of the field enhancement (F.E. in arbitrary units) seen between nanoparticles

F.E.~
$$[E_0 + q_{\text{eff}}(1 - e^{-\lambda D})]e^{-\alpha D}$$
 (1)

where E_0 is a parameter related to the strength of the incident/driving field and α is the damping coefficient.

We presented the results in arbitrary units to stress that this expression is meant solely as a phenomenological description of the relevant physics. Since the geometry and physical dimensions of the experimental system greatly affects the parameters used, we did not attempt to derive the values of these parameters from first-principles but rather fitted them

according to the experimental results in order to see if a qualitative analysis of the fit matches our intuition of the parameters. The experimental data from three different nanoparticle composites (TiO₂, WO₃ and SiO₂) were fit according to this model and the results are shown in Figure. 6a. The plot fits show the different physical processes going on. For example, consider the plot for WO₃; at D = 1 nm tunneling dominates, which reduces the measured field enhancement compared to D = 3 nm where tunneling is less probable. The same can be seen for TiO2. At large separation tunneling no longer has a big effect, but energy loss to the surrounding medium lowers the peak absorption. We thus identified an optimal separation distance for maximum field strength between the particles. In the case of SiO₂ the tunneling barrier is so high that we did not see an optimal separation. The fit for TiO₂ is not as exact as the others but it still qualitatively agrees with the experiment showing an optimal separation between 3 and 4 nm. Indeed, the fits show a proper ordering of the tunneling barrier height for the three materials.

It has been shown that the plasmon frequency of gold nanoparticles redshifts with an increase in particle size. 61 The plasmon frequency for metal nanoparticles coated with a dielectric also exhibit redshifts with increased coating thickness. 69,70 The redshift is believed to be due to polarization of the surrounding medium which decreases the surface charge on the nanoparticle, which in turn reduces the restoring force of the plasmon oscillations.⁷¹ Our observed redshift of the single nanoparticle plasmon mode due to the proximity of the other nanoparticle is also consistent with this explanation. The further apart the nanoparticles are from each other the more dielectric material separates them, i.e., the more screening both nanoparticles feel. Consequently, we expect the plasmon frequency to be dependent on the inverse of the dielectric constant (ϵ) of the coating material. Furthermore, redshift is also caused by "phase retardation" which works as follows: the separation between the nanoparticles leads to a phase shift of the electromagnetic wave at the neighboring nanoparticle compared to the plasmon which emitted the wave. The charge oscillation on each nanoparticle will consequently be ahead in phase from the electromagnetic wave coming from the other nanoparticle leading to a decrease in phase velocity and therefore a redshift in the plasmon frequency. This redshift is expected to be linearly dependent on the time it takes a signal to travel from one particle to the other which is proportional to nD where n is the index of refraction of the dielectric coating material (recall the speed of electromagnetic radiation in a medium is v = c/n). The index of refraction of the dielectric coating material were obtained by measuring control samples with ellipsometry after ALD deposition. The values are 2.59, 2.20, 1.45 for TiO₂, WO₃, and SiO₂, respectively. We therefore expect the redshift to be characterized by the following relationship:

$$\lambda_{\max} = A \frac{n}{\epsilon} D + \lambda_0$$

where A is some proportionality constant that depends on the geometry of the system and not on the material used for the coating. Finally, recall that for nonmagnetic materials $\epsilon = n^2$, thus

$$\lambda_{\text{max}} = A \frac{D}{n} + \lambda_0 \tag{2}$$

The measured red shift is shown in Figure 7b as a function of D/n. We see that the geometric parameter (slope of lines of best fit) matches closely for all three systems as expected.

We should mention that several experiments have found blue shift for increasing particle separation but at larger separations than shown here. This stands to reason since the coupling between nanoparticles will decay with increased distance and therefore we should expect the rate of redshift to decrease at some point and eventually turn to blue shift in order to restore the single nanoparticle plasmon frequency (λ_0) . We saw a linear redshift up to the maximum separation considered in the experiment for all three materials but judging by the rate of decrease in measured field strength between the particles we would not expect the redshift to continue according to the above model for much more than 10 nm separation.

CONCLUSIONS

In summary, we created a technology to fabricate down to subnanometer gap plasmonic structures with high precision, high reliability, and high throughput deterministically. Precisely controlled nanogap arrays down to subnanometer in large area can be produced using collapsible nanofingers. We experimentally proved and observed optimal gap sizes for gap plasmonic structures with different dielectric spacers. Meanwhile, we also demonstrated direct control of tunneling strength by simply changing the material between gold nanoparticles, and showed that lower tunneling barrier heights result in larger optimal gap sizes. This technology enables us to put active materials at the hottest part of optimally designed gap plasmonic hot spot, which is a great platform for various further applications.

METHODS

Sample Preparation. As shown in Figure 2a, the first layer was a 600 nm thick UV nanoimprint resist (I-UVP 15% concentration, EZImprinting Inc.) spin-coated (11 s at 2000 rpm) onto a glass substrate and cured under 4 mW/cm² i-line (365 nm) UV exposure for 5 min. Then, the second layer was a 100 nm lift-off underlayer (I-ULP 3.5% concentration, EZImprinting Inc.) spin-coated (40 s at 4000 rpm) and baked at 120 °C for 5 min, which served as the adhesive layer. Another 100 nm UV nanoimprint resist (I-UVP 4.1% concentration, EZImprinting Inc.) layer was spin-coated (10 s at 2500 rpm) onto the lift-off underlayer, and a subsequent NIL step (Figure 2b) was performed using the previous daughter mold to form the original hole pattern. We etched the residual UV imprint resist layer and underlying lift-off underlayer by reactive-ion etching (RIE, Oxford PlasmaPro 100). Then, 50 nm gold on top of 2 nm titanium (adhesive layer) was deposited onto the sample by e-beam evaporation (Temescal BJD-1800 E-Beam Evaporator) at slightly off-normal incidence. Next, we lifted off the lift-off underlayer and layers above it using a hot acetone bath, and patterned gold caps array were left on the thick UV imprint resist, as shown in Figure 2c. Au nanoparticles were formed, which also served as etching mask for the following steps. Because the evaporation is at slightly off-normal incidence, the gold nanoparticles are not strictly symmetric. This is why the fingers can collapse in a dimer fashion. Then we etched the uncovered UV imprint resist by RIE to 350 nm deep and obtained high aspect ratio polymer nanofingers with Au nanoparticles on the tip (Figure 2d). The samples were then covered by dielectric layers of variable thickness after a plasma enhanced ALD process (Oxford PlasmaPro 100), as shown in Figure 2e. Since the ALD film has excellent conformity, monitor samples with flat Au top surface were used during the deposition process for accurate measurement of ALD film thickness by ellipsometry (VASE ellipsometer).

SEM TEM and EDS Measurements. SEM images were taken by JEOL JSM 7001. Eight kilovolt accelerating voltage was used in the

imaging. In Figure 3a, the viewing angle is 40° tilt from surface normal and the inset image shows cross section. Figure 3b shows the top view and the viewing angle of the inset image is 20° tilt from surface normal. Samples for TEM cross section were prepared by focused ion beam (FIB) in the direction paralleled to dimer direction.

Absorption Spectroscopy. All absorption spectra were obtained by a UV-Vis-NIR spectrophotometer (PerkinElmer Lambda 950) by shining parallel polarized (dimer axis) light onto the sample at normal incidence. Taking into account the compensation for the background signal, the absorption spectra of the sample before the nanofingers collapsed were also measured in the same setup and deducted from the final results. The incident light power was fixed for all the measurements.

AUTHOR INFORMATION

Corresponding Author

*E-mail: wu.w@usc.edu.

ORCID ®

Boxiang Song: 0000-0002-4946-2738 Yuhan Yao: 0000-0001-7392-7147

Adam M. Schwartzberg: 0000-0001-6335-0719

Notes

The authors declare no competing financial interest.

ACKNOWLEDGMENTS

We thank Dr. A. F. Levi for helpful discussion. W. Wu would like to acknowledge support from NSF CMMI-1635612. S. Haas would like to acknowledge support from the Department of Energy under Grant No. DE-FG02-05ER46240. S. B. Cronin would like to acknowledge support from the Air Force Office of Scientific Research (AFOSR) Grant No. FA9550-15-1-0184. Fanxin Liu would like to acknowledge support from National Natural Science Foundation of China under Grant No. 11574270 and Natural Science Foundation of Zhejiang Province under Grant No. LY15A040005. Work at the Molecular Foundry was supported by the Office of Science, Office of Basic Energy Sciences, of the U.S. Department of Energy under Contract No. DE-AC02-05CH11231.

REFERENCES

- (1) Linic, S.; Christopher, P.; Ingram, D. B. Plasmonic-Metal Nanostructures for Efficient Conversion of Solar to Chemical Energy. *Nat. Mater.* **2011**, *10*, 911–921.
- (2) Atwater, H. A.; Polman, A. Plasmonics for Improved Photovoltaic Devices. *Nat. Mater.* **2010**, *9*, 205–213.
- (3) Mühlschlegel, P.; Eisler, H.-J.; Martin, O.; Hecht, B.; Pohl, D. Resonant Optical Antennas. *Science* **2005**, *308*, 1607–1609.
- (4) Novotny, L.; Van Hulst, N. Antennas for Light. *Nat. Photonics* **2011**, *5*, 83–90.
- (5) Giannini, V.; Fernández-Domínguez, A. I.; Heck, S. C.; Maier, S. A. Plasmonic Nanoantennas: Fundamentals and Their Use in Controlling the Radiative Properties of Nanoemitters. *Chem. Rev.* **2011**, *111*, 3888–3912.
- (6) Alvarez-Puebla, R.; Liz-Marzán, L. M.; García de Abajo, F. J. Light Concentration at the Nanometer Scale. *J. Phys. Chem. Lett.* **2010**, *1*, 2428–2434.
- (7) Ansell, D.; Radko, I.; Han, Z.; Rodriguez, F.; Bozhevolnyi, S.; Grigorenko, A. Hybrid Graphene Plasmonic Waveguide Modulators. *Nat. Commun.* **2015**, *6*, 8846.
- (8) Song, J.; Huang, P.; Duan, H.; Chen, X. Plasmonic Vesicles of Amphiphilic Nanocrystals: Optically Active Multifunctional Platform for Cancer Diagnosis and Therapy. *Acc. Chem. Res.* **2015**, *48*, 2506–2515.

(9) Stewart, M. E.; Anderton, C. R.; Thompson, L. B.; Maria, J.; Gray, S. K.; Rogers, J. A.; Nuzzo, R. G. Nanostructured Plasmonic Sensors. *Chem. Rev.* **2008**, *108*, 494–521.

- (10) Schuller, J. A.; Barnard, E. S.; Cai, W.; Jun, Y. C.; White, J. S.; Brongersma, M. L. Plasmonics for Extreme Light Concentration and Manipulation. *Nat. Mater.* **2010**, *9*, 193–204.
- (11) Halas, N. J.; Lal, S.; Chang, W.-S.; Link, S.; Nordlander, P. Plasmons in Strongly Coupled Metallic Nanostructures. *Chem. Rev.* **2011**, *111*, 3913–3961.
- (12) Pasquale, A. J.; Reinhard, B. r. M.; Dal Negro, L. Engineering Photonic—Plasmonic Coupling in Metal Nanoparticle Necklaces. *ACS Nano* **2011**, *5*, 6578—6585.
- (13) Kelly, K. L.; Coronado, E.; Zhao, L. L.; Schatz, G. C. The Optical Properties of Metal Nanoparticles: The Influence of Size, Shape, and Dielectric Environment. *J. Phys. Chem. B* **2003**, *107*, 668–677.
- (14) Marinica, D. C.; Kazansky, A. K.; Nordlander, P.; Aizpurua, J.; Borisov, A. G. Quantum Plasmonics: Nonlinear Effects in the Field Enhancement of a Plasmonic Nanoparticle Dimer. *Nano Lett.* **2012**, *12*, 1333–1339.
- (15) Tame, M. S.; McEnery, K.; Özdemir, Ş.; Lee, J.; Maier, S.; Kim, M. Quantum Plasmonics. *Nat. Phys.* **2013**, *9*, 329–340.
- (16) Esteban, R.; Borisov, A. G.; Nordlander, P.; Aizpurua, J. Bridging Quantum and Classical Plasmonics with a Quantum-Corrected Model. *Nat. Commun.* **2012**, *3*, 825.
- (17) Nordlander, P.; Oubre, C.; Prodan, E.; Li, K.; Stockman, M. Plasmon Hybridization in Nanoparticle Dimers. *Nano Lett.* **2004**, *4*, 899–903.
- (18) García-Martín, A.; Ward, D. R.; Natelson, D.; Cuevas, J. C. Field Enhancement in Subnanometer Metallic Gaps. *Phys. Rev. B: Condens. Matter Mater. Phys.* **2011**, 83, 193404.
- (19) Savage, K. J.; Hawkeye, M. M.; Esteban, R.; Borisov, A. G.; Aizpurua, J.; Baumberg, J. J. Revealing the Quantum Regime in Tunnelling Plasmonics. *Nature* **2012**, *491*, 574–577.
- (20) Zhu, W.; Crozier, K. B., Quantum Mechanical Limit to Plasmonic Enhancement as Observed by Surface-Enhanced Raman Scattering. *Nat. Commun.* **2014**, 5.522810.1038/ncomms6228
- (21) Yang, L.; Wang, H.; Fang, Y.; Li, Z. Polarization State of Light Scattered from Quantum Plasmonic Dimer Antennas. *ACS Nano* **2016**, *10*, 1580–1588.
- (22) Chen, Y.; Bi, K.; Wang, Q.; Zheng, M.; Liu, Q.; Han, Y.; Yang, J.; Chang, S.; Zhang, G.; Duan, H. Rapid Focused Ion Beam Milling Based Fabrication of Plasmonic Nanoparticles and Assemblies *via* "Sketch and Peel" Strategy. *ACS Nano* **2016**, *10*, 11228–11236.
- (23) Forati, E.; Dill, T. J.; Tao, A. R.; Sievenpiper, D., Photoemission-Based Microelectronic Devices. *Nat. Commun.* **2016**, 7.1339910.1038/ncomms13399
- (24) Duan, H.; Hu, H.; Kumar, K.; Shen, Z.; Yang, J. K. Direct and Reliable Patterning of Plasmonic Nanostructures with Sub-10-Nm Gaps. *ACS Nano* **2011**, *5*, 7593–7600.
- (25) George, S. M. Atomic Layer Deposition: An Overview. Chem. Rev. 2010, 110, 111–131.
- (26) Elam, J.; Routkevitch, D.; Mardilovich, P.; George, S. Conformal Coating on Ultrahigh-Aspect-Ratio Nanopores of Anodic Alumina by Atomic Layer Deposition. *Chem. Mater.* **2003**, *15*, 3507–3517.
- (27) Standridge, S. D.; Schatz, G. C.; Hupp, J. T. Toward Plasmonic Solar Cells: Protection of Silver Nanoparticles *via* Atomic Layer Deposition of TiO₂. *Langmuir* **2009**, *25*, 2596–2600.
- (28) Tan, S. F.; Wu, L.; Yang, J. K.; Bai, P.; Bosman, M.; Nijhuis, C. A. Quantum Plasmon Resonances Controlled by Molecular Tunnel Junctions. *Science* **2014**, 343, 1496–1499.
- (29) Liu, H.; Yao, Y.; Wang, Y.; Wu, W. Full-Color Reflective Display System Based on High Contrast Gratings. J. Vac. Sci. Technol., B: Nanotechnol. Microelectron.: Mater., Process., Meas., Phenom. 2014, 32, 06FE04.
- (30) Savas, T.; Schattenburg, M.; Carter, J.; Smith, H. I. Large-Area Achromatic Interferometric Lithography for 100 Nm Period Gratings and Grids. *J. Vac. Sci. Technol., B: Microelectron. Process. Phenom.* **1996**, 14, 4167–4170.

(31) Yao, Y.; Wang, Y.; Liu, H.; Li, Y.; Song, B.; Wu, W. Line Width Tuning and Smoothening for Periodical Grating Fabrication in Nanoimprint Lithography. *Appl. Phys. A: Mater. Sci. Process.* **2015**, 121, 399–403.

- (32) Chou, S. Y.; Krauss, P. R.; Renstrom, P. J. Nanoimprint Lithography. J. Vac. Sci. Technol., B: Microelectron. Process. Phenom. 1996, 14, 4129–4133.
- (33) Yao, Y.; Liu, H.; Wang, Y.; Li, Y.; Song, B.; Bratkovsk, A.; Wang, S.-Y.; Wu, W. Nanoimprint Lithography: An Enabling Technology for Nanophotonics. *Appl. Phys. A: Mater. Sci. Process.* **2015**, *121*, 327–333.
- (34) Gates, B. D.; Xu, Q.; Stewart, M.; Ryan, D.; Willson, C. G.; Whitesides, G. M. New Approaches to Nanofabrication: Molding, Printing, and Other Techniques. *Chem. Rev.* **2005**, *105*, 1171–1196.
- (35) Colburn, M.; Johnson, S. C.; Stewart, M. D.; Damle, S.; Bailey, T. C.; Choi, B.; Wedlake, M.; Michaelson, T. B.; Sreenivasan, S.; Ekerdt, J. G. In Step and Flash Imprint Lithography: A New Approach to High-Resolution Patterning, Microlithography'99, International Society for Optics and Photonics; 1999; pp 379–389.
- (36) Ou, F. S.; Hu, M.; Naumov, I.; Kim, A.; Wu, W.; Bratkovsky, A. M.; Li, X.; Williams, R. S.; Li, Z. Hot-Spot Engineering in Polygonal Nanofinger Assemblies for Surface Enhanced Raman Spectroscopy. *Nano Lett.* **2011**, *11*, 2538–2542.
- (37) Chandra, D.; Yang, S. Capillary-Force-Induced Clustering of Micropillar Arrays: Is It Caused by Isolated Capillary Bridges or by the Lateral Capillary Meniscus Interaction Force? *Langmuir* **2009**, 25, 10430–10434.
- (38) Kotera, M.; Ochiai, N. Three-Dimensional Simulation of Resist Pattern Deformation by Surface Tension at the Drying Process. *Microelectron. Eng.* **2005**, *78*, 515–520.
- (39) Chini, S. F.; Amirfazli, A. Understanding Pattern Collapse in Photolithography Process Due to Capillary Forces. *Langmuir* **2010**, *26*, 13707–13714.
- (40) Duan, H.; Berggren, K. K. Directed Self-Assembly at the 10 Nm Scale by Using Capillary Force-Induced Nanocohesion. *Nano Lett.* **2010**, *10*, 3710–3716.
- (41) Zhang, R.; Zhang, Y.; Dong, Z.; Jiang, S.; Zhang, C.; Chen, L.; Zhang, L.; Liao, Y.; Aizpurua, J.; Luo, Y. e.; Yang, J. L.; Hou, J. G. Chemical Mapping of a Single Molecule by Plasmon-Enhanced Raman Scattering. *Nature* **2013**, *498*, 82–86.
- (42) Li, J. F.; Huang, Y. F.; Ding, Y.; Yang, Z. L.; Li, S. B.; Zhou, X. S.; Fan, F. R.; Zhang, W.; Zhou, Z. Y.; Ren, B.; Wu, D. Y.; Wang, Z. L.; Tian, Z. Q. Shell-Isolated Nanoparticle-Enhanced Raman Spectroscopy. *Nature* **2010**, 464, 392–395.
- (43) Zhu, Z.; Yan, Z.; Zhan, P.; Wang, Z. Large-Area Surface-Enhanced Raman Scattering-Active Substrates Fabricated by Femtosecond Laser Ablation. *Sci. China: Phys., Mech. Astron.* **2013**, *56*, 1806—1809.
- (44) Schnell, M.; Garcia-Etxarri, A.; Huber, A.; Crozier, K.; Aizpurua, J.; Hillenbrand, R. Controlling the near-Field Oscillations of Loaded Plasmonic Nanoantennas. *Nat. Photonics* **2009**, *3*, 287–291.
- (45) Su, K.-H.; Wei, Q.-H.; Zhang, X.; Mock, J.; Smith, D. R.; Schultz, S. Interparticle Coupling Effects on Plasmon Resonances of Nanogold Particles. *Nano Lett.* **2003**, *3*, 1087–1090.
- (46) Lim, D.-K.; Jeon, K.-S.; Kim, H. M.; Nam, J.-M.; Suh, Y. D. Nanogap-Engineerable Raman-Active Nanodumbbells for Single-Molecule Detection. *Nat. Mater.* **2010**, *9*, 60–67.
- (47) Lim, D.-K.; Jeon, K.-S.; Hwang, J.-H.; Kim, H.; Kwon, S.; Suh, Y. D.; Nam, J.-M. Highly Uniform and Reproducible Surface-Enhanced Raman Scattering from DNA-Tailorable Nanoparticles with 1-Nm Interior Gap. *Nat. Nanotechnol.* **2011**, *6*, 452–460.
- (48) Oh, J.-W.; Lim, D.-K.; Kim, G.-H.; Suh, Y. D.; Nam, J.-M. Thiolated DNA-Based Chemistry and Control in the Structure and Optical Properties of Plasmonic Nanoparticles with Ultrasmall Interior Nanogap. J. Am. Chem. Soc. 2014, 136, 14052—14059.
- (49) Jain, P. K.; Huang, W.; El-Sayed, M. A. On the Universal Scaling Behavior of the Distance Decay of Plasmon Coupling in Metal Nanoparticle Pairs: A Plasmon Ruler Equation. *Nano Lett.* **2007**, *7*, 2080–2088.

(50) Romero, I.; Aizpurua, J.; Bryant, G. W.; De Abajo, F. J. G. Plasmons in Nearly Touching Metallic Nanoparticles: Singular Response in the Limit of Touching Dimers. *Opt. Express* **2006**, *14*, 9988–9999.

- (51) McMahon, J. M.; Gray, S. K.; Schatz, G. C. Optical Properties of Nanowire Dimers with a Spatially Nonlocal Dielectric Function. *Nano Lett.* **2010**, *10*, 3473–3481.
- (52) David, C.; García de Abajo, F. J. Spatial Nonlocality in the Optical Response of Metal Nanoparticles. *J. Phys. Chem. C* **2011**, *115*, 19470–19475.
- (53) Teperik, T. V.; Nordlander, P.; Aizpurua, J.; Borisov, A. G. Quantum Effects and Nonlocality in Strongly Coupled Plasmonic Nanowire Dimers. *Opt. Express* **2013**, *21*, 27306–27325.
- (54) García de Abajo, F. J. Nonlocal Effects in the Plasmons of Strongly Interacting Nanoparticles, Dimers, and Waveguides. *J. Phys. Chem. C* **2008**, *112*, 17983–17987.
- (55) Dong, T.; Ma, X.; Mittra, R. Optical Response in Subnanometer Gaps Due to Nonlocal Response and Quantum Tunneling. *Appl. Phys. Lett.* **2012**, *101*, 233111.
- (56) Toscano, G.; Raza, S.; Xiao, S.; Wubs, M.; Jauho, A.-P.; Bozhevolnyi, S. I.; Mortensen, N. A. Surface-Enhanced Raman Spectroscopy: Nonlocal Limitations. *Opt. Lett.* **2012**, *37*, 2538–2540.
- (57) Teperik, T. V.; Nordlander, P.; Aizpurua, J.; Borisov, A. G. Robust Subnanometric Plasmon Ruler by Rescaling of the Nonlocal Optical Response. *Phys. Rev. Lett.* **2013**, *110*, 263901.
- (58) Wu, H.; Wang, L. S. Electronic Structure of Titanium Oxide Clusters: TiO_y (y=1-3) and (TiO_2)_n (n=1-4). *J. Chem. Phys.* **1997**, 107, 8221–8228.
- (59) Walter, C.; Hertzler, C.; Devynck, P.; Smith, G.; Peterson, J. Photodetachment of WO₃: The Electron Affinity of WO₃. *J. Chem. Phys.* **1991**, *95*, 824–827.
- (60) Pantelides, S. T. The Physics of SiO₂ and Its Interfaces: Proceedings of the International Topical Conference on the Physics of SiO₂ and Its Interfaces Held at the IBM Thomas J. Waston Research Center, Yorktown Heights, New York, March 22–24, 1978; Elsevier: 2013.
- (61) Link, S.; El-Sayed, M. A. Size and Temperature Dependence of the Plasmon Absorption of Colloidal Gold Nanoparticles. *J. Phys. Chem. B* **1999**, *103*, 4212–4217.
- (62) Link, S.; El-Sayed, M. A. Shape and Size Dependence of Radiative, Non-Radiative and Photothermal Properties of Gold Nanocrystals. *Int. Rev. Phys. Chem.* **2000**, *19*, 409–453.
- (63) Born, M.; Wolf, E. Principles of Optics: Electromagnetic Theory of Propagation, Interference and Diffaction of Light; Pergamon Press, 1959.
- (64) Fan, X.; Zheng, W.; Singh, D. J. Light Scattering and Surface Plasmons on Small Spherical Particles. *Light: Sci. Appl.* **2014**, *3*, e179.
- (65) García de Abajo, F. J. Optical Excitations in Electron Microscopy. Rev. Mod. Phys. 2010, 82, 209–275.
- (66) Nordlander, P.; Oubre, C.; Prodan, E.; Li, K.; Stockman, M. I. Plasmon Hybridization in Nanoparticle Dimers. *Nano Lett.* **2004**, *4*, 899–903.
- (67) Lassiter, J. B.; Aizpurua, J.; Hernandez, L. I.; Brandl, D. W.; Romero, I.; Lal, S.; Hafner, J. H.; Nordlander, P.; Halas, N. J. Close Encounters between Two Nanoshells. *Nano Lett.* **2008**, *8*, 1212–1218.
- (68) Zuloaga, J.; Prodan, E.; Nordlander, P. Quantum Description of the Plasmon Resonances of a Nanoparticle Dimer. *Nano Lett.* **2009**, *9*, 887–891.
- (69) Lebedev, V.; Vitukhnovsky, A.; Yoshida, A.; Kometani, N.; Yonezawa, Y. Absorption Properties of the Composite Silver/Dye Nanoparticles in Colloidal Solutions. *Colloids Surf., A* **2008**, 326, 204–209.
- (70) Quinsaat, J. E. Q.; Nüesch, F. A.; Hofmann, H.; Opris, D. M. Dielectric Properties of Silver Nanoparticles Coated with Silica Shells of Different Thicknesses. *RSC Adv.* **2013**, *3*, 6964–6971.
- (71) Cheng, P.; Bao, J.; Wu, L.; Li, X.; Zhao, H.; Zhu, R.; Wang, J.; Li, D. Surface Plasmon Response of Metal Spherical Nanoshells Coated with Dielectric Overlayer. *Chem. Phys. Lett.* **2013**, *587*, 40–44.